JOC The Journal of Organic Chemistry

Article

pubs.acs.org/joc

Atropisomers of Hindered Triarylisocyanurates: Structure, Conformation, Stereodynamics, and Absolute Configuration

Lodovico Lunazzi, Michele Mancinelli, and Andrea Mazzanti*

Department of Organic Chemistry "A. Mangini", University of Bologna, Viale Risorgimento 4, I-40136 Bologna, Italy

Supporting Information

ABSTRACT: The *syn* and *anti* diastereoisomers of some 1,3,5-triarylisocyanurate derivatives were isolated and their configuration assigned by NOE experiments and by X-ray diffraction. The kinetics of the *syn*/*anti* interconversion were determined, and the experimental activation energies matched satisfactorily the values predicted by DFT computations. Low-temperature NMR spectra were employed to determine the rotation barrier of N-bonded unhindered aryl substituents: these barriers, too, are satisfactorily reproduced by DFT computations. In the case of racemic diastereoisomers, the two expected enantiomers (atropisomers) were isolated by enantioselective HPLC and the absolute configuration established by DFT simulation of the electronic and vibrational circular dichroism spectra.

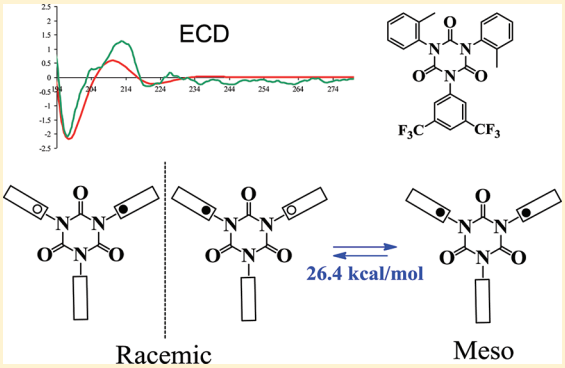

INTRODUCTION

Isocyanurate (1,3,5-triazinane-2,4,6-trione) is obtained from the cyclotrimerization of isocyanate[1] and is used to modify the physical properties of polyurethane foams and coating materials.[2] Polymeric blends of isocyanurates show increased thermal resistance, flame retardation, chemical resistance, and film-forming characteristics.[3] For example, triaryl isocyanurates are often used as activators for the polymerization and postpolymerization of ε-caprolactam in the production of nylons with high melt viscosities.[4] Triallyl isocyanurate has been used in the preparation of flame-retardant laminating materials for electrical devices as well as in the preparation of copolymer resins that are water-resistant, transparent, and impact-resistant.[5] Recently, the rigid structure of isocyanurate has found interesting application in the fields of chiral discrimination and low toxicity drug delivery.[6] Isocyanurate is a suitable framework molecule for designing host molecules to realize chiral recognition, since the multistereogenic centers on the N-substituents are organized on an inflexible six-membered isocyanurate ring and then work cooperatively.[6]

When a six-membered cyclic planar moiety (e.g., a benzene ring) bears a number of bulky aromatic substituents without a local C_2 symmetry axis, a number of stereoisomeric forms can exist. This is because the substituents undergo a restricted rotation process that creates a number of out-of-plane structures. When these aryl groups are sufficiently bulky (for example, bearing an *ortho* substituent) and they are bonded to positions 1,2 (i.e., vicinal substituents), the corresponding stereoisomers are often stable enough to be physically separable.[7−12] On the other hand, if the six-membered scaffold bears the aryl rings in the *meta* or *para* positions, the interconversion of the stereoisomers is usually too fast to allow a physical separation; they can nonetheless be detected by NMR spectroscopy, usually at low temperature.[7,8,12−15]

RESULTS AND DISCUSSION

Isocyanurate is a six-membered ring and, although not aromatic, is nevertheless a rather rigid system. Quite surprisingly, DFT calculations at the B3LYP/6-31G(d) level predict that the stereoisomers arising from the restricted rotation of the aryl groups in 1,3,5-tri-*ortho*-tolyl-isocyanurate (i.e., 1,3,5-tri-*ortho*-tolyl-1,3,5-triazinane-2,4,6-trione) **1** (see Scheme 1) have an interconversion barrier as high as 25.9

Scheme 1

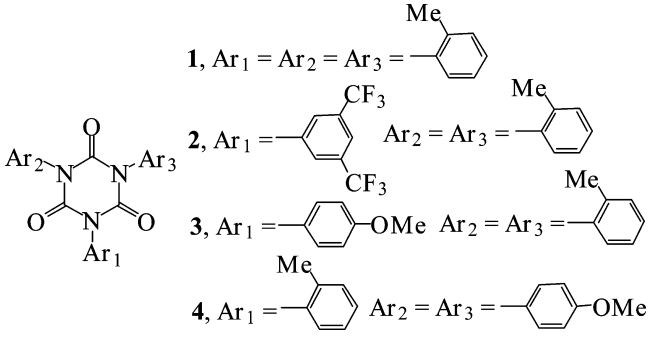

kcal mol^{-1}. This value suggests that it should be possible to physically separate these forms, despite the fact that the *ortho*-tolyl substituents are not in a vicinal position. To verify such a prediction, compound **1** was prepared by reacting 1-isocyanato-

Received: January 25, 2012
Published: March 2, 2012

   dx.doi.org/10.1021/jo300192n | J. Org. Chem. 2012, 77, 3373−3380

2-methylbenzene with a catalytic amount of potassium acetate at +130 °C.

The reaction actually provided two diastereoisomers (in a 73:27 ratio) that could be separated by semipreparative HPLC. The *anti* structure with C_s symmetry (Scheme 2) was assigned

Scheme 2. DFT Computed Structures of the Diastereoisomers of 1 and 2 with the Relative Energies (E) in kcal mol^{-1}

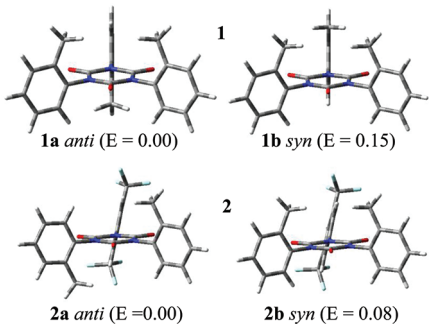

to the major diastereoisomer (**1a**) because its NMR spectrum displayed two methyl signals with a 2:1 intensity ratio.

On the other hand, the minor diastereoisomer showed a single NMR methyl signal and was, therefore, identified as having the *syn* structure **1b** (C_{3v} symmetry).

When the isolated minor diastereoisomer *syn* (**1b**) was kept at +70 °C in acetonitrile, the major *anti* diastereoisomer (**1a**) was generated and its population increased, until a 71:29 *anti*:*syn* ratio was reached at the equilibrium. This ratio is essentially the same as that obtained in the synthesis of **1**, thus indicating that the reaction is under thermodynamic control. The kinetics of the interconversion process (see Figure S1 of the Supporting Information) was followed by monitoring the HPLC trace as a function of time and provided a barrier for the **1b** (C_{3v}) to **1a** (C_s) interconversion equal to 26.6 kcal mol^{-1} (the barrier from the major **1a** to the minor **1b** is 27.2 kcal mol^{-1}, as in Table 1).

Table 1. Free Energies of Activation ($\Delta G^{\ddagger}$) for the Dynamic Processes Measured in 1−4 and, in Parentheses, the DFT Computed $\Delta E^{\ddagger}$ Values, Both in kcal mol^{-1}

	aryl−N rotation	
compd	*syn*/*anti* interconversion[a]	homomerization[b]
1	26.6 27.2 (25.9)	[c]
2	26.4 26.5 (25.4)	10.8 (9.7)
3	26.6$_5$ 26.8 (26.0)	12.2 (10.8)
4	[c]	12.3 (10.5)

[a]The first column refers to the measured barrier from the less to the more stable and the second from the more to the less stable form. The values in parentheses (third column) refer to the computed barrier from the more to the less stable form. [b]Barriers for rotation of the aryl rings without *ortho* substituent. [c]Not measurable (see text).

It should be also pointed out that the structure of the major *anti* (**1a**) diastereoisomer is 3-fold degenerate in contrast to **1b**; thus its larger proportion is mainly due to a statistic entropy factor (RT ln 3). If this correction is considered, the thermodynamic stabilities of the two forms are quite similar, a result that agrees with DFT calculations predicting a negligible energy difference (0.15 kcal mol^{-1}) between **1a** and **1b** (Scheme 2).

The barrier measured in the case of **1** confirms the prediction of the DFT calculations, and its large value implies that, in derivatives where one of the three *ortho*-tolyl groups is replaced by another aromatic substituent having a local 2-fold N−Ar symmetry axis (C_2), the *syn* and *anti* diastereoisomers would correspond, respectively, to a meso (C_s) and to a racemic form (C_2): the latter should be, therefore, separable into a pair of stable conformational enantiomers (atropisomers).

To verify this point, derivative **2**, bearing in position 1 the 3,5-bis(trifluoromethyl)phenyl group, was prepared and the two diastereoisomers were obtained in a 47:53 proportion (**2a** and **2b**, respectively). They could be separated by semipreparative HPLC, and the corresponding theoretical structures, as obtained by DFT calculations, are displayed in Scheme 2. The pure major diastereoisomer **2b** was kept at +80 °C, and its interconversion into the minor isomer **2a** was followed by NMR as a function of time. The ratio obtained at the equilibrium (52:48) was nearly equal to that obtained from the synthetic process (53:47), suggesting a reaction under thermodynamic control. The kinetics of this process (Figure S2 of the Supporting Information) yielded a value for the interconversion barrier of 26.5 kcal mol^{-1}, to be compared with the DFT theoretical barrier of 25.4 kcal mol^{-1} (Table 1).

The NMR spectra of **2a** and **2b**, unlike the cases of **1a** and **1b**, do not allow unambiguous assignment of the *syn* or *anti* configuration. Therefore, we resorted to a previously reported NOE experiment to achieve this assignment.[16] In a CD_3CN solution containing the reaction mixture of **2a** and **2b**, the pairs of ^{13}C satellites[17] of both methyl lines were simultaneously irradiated. As shown in Figure 1, the lower-field methyl line (2.337 ppm) of the second eluted (slightly major) compound **2b** yields an NOE effect, indicating that this line belongs to the *syn* (meso) diastereoisomer, where the hydrogens of the two methyl groups are sufficiently close to experience a reciprocal intensity enhancement.[18]

On the contrary, irradiation of the ^{13}C satellites does not produce a NOE effect on the higher-field methyl line (2.331 ppm): the corresponding (slightly minor) diastereoisomer **2a** has, consequently, the *anti* (racemic) configuration, where the hydrogens of the two methyl groups are too far apart[18] to yield such an enhancement.

An independent check of this assignment was obtained by monitoring the effects on the spectral lines of the third aryl ring when the temperature is lowered. At ambient temperature, the rotation of the 3,5-bis(trifluoromethyl)phenyl ring is fast; thus the different symmetries of the two diastereoisomers **2a** and **2b** cannot be distinguished by NMR. However, when the spectrum is recorded at a temperature sufficiently low as to freeze this rotation, two possible situations might, in principle, be encountered:

(i) If the ground-state conformation of the 3,5-bis(trifluoromethyl)phenyl ring is coplanar with that of isocyanurate, the low-temperature spectrum will not change so that a single signal[19] for the two *ortho* hydrogens of the 3,5-bis(trifluoromethyl)phenyl substituent would still be observed in each diastereoisomer, since, in both cases, they remain isochronous (they are homotopic in the *anti* and enantiotopic in the *syn* form). If such a situation occurs, this experiment would not allow a structural assignment.

dx.doi.org/10.1021/jo300192n | J. Org. Chem. 2012, 77, 3373−3380

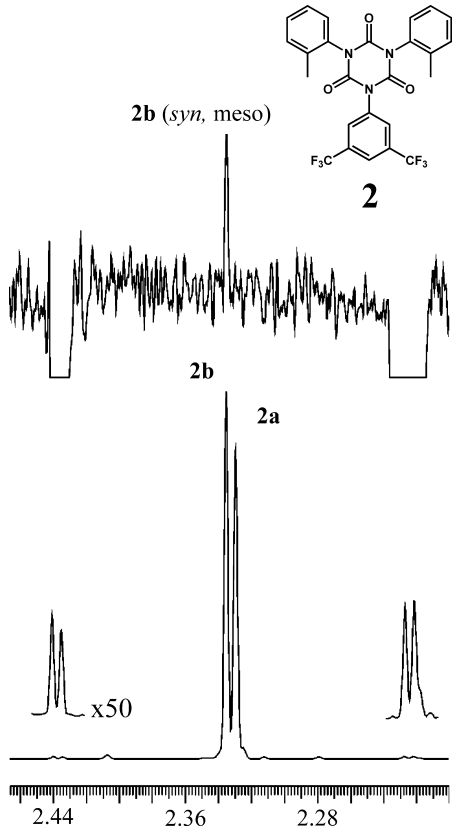

Figure 1. Bottom: methyl lines (600 MHz in CD_3CN) of the 53:47 mixture of **2b** and **2a** with the 50-fold enhanced ^{13}C satellites in the inset (the small signals at 2.41 and 2.28 ppm are impurities of the solvent). Top: spectrum resulting from the simultaneous irradiation of the ^{13}C satellites, yielding the NOE effect solely for the downfield line of diastereoisomer **2b** (*syn*, meso).

(ii) If, on the contrary, the adopted conformation has the 3,5-bis(trifluoromethyl)phenyl ring orthogonal to that of isocyanurate, as predicted by calculations, the frozen rotation would make the mentioned *ortho* hydrogens diastereotopic in the *syn* (meso), but enantiotopic, thus isochronous, in the *anti* (racemic) diastereoisomer.

The first eluted diastereoisomer **2a** displays a single ^1H line for the *ortho* hydrogens of the 3,5-bis(trifluoromethyl)phenyl ring[19] at any temperature (down to −100 °C), as expected for the *anti* (racemic) configuration. On the contrary, the corresponding line[19] of the second eluted diastereoisomer **2b** broadens on cooling, decoalesces, and eventually splits, at −87 °C, into a pair of equally intense signals separated by 26 Hz (at 600 MHz), as shown in Figure 2. By line-shape simulation, the rate constants were determined and a rotation barrier of 10.8 kcal mol^{-1} was obtained (the DFT calculated barrier is 9.7 kcal mol^{-1}, as in Table 1). This confirms that the second eluted diastereoisomer **2b** has the *syn* (meso) configuration and also that the 3,5-bis(trifluoromethyl)phenyl ring is not coplanar with the isocyanurate plane. The calculations predict indeed that the 3,5-bis(trifluoromethyl)phenyl substituent is twisted with respect to the isocyanurate moiety in both **2a** *anti* (racemic) and **2b** *syn* (meso) and that the *anti* diastereoisomer **2a** appears to be slightly more stable (by 0.08 kcal mol^{-1}) than the *syn* **2b** (Scheme 2).

In view of the approximations of these calculations, such a small difference does not contradict the experimental ratio at

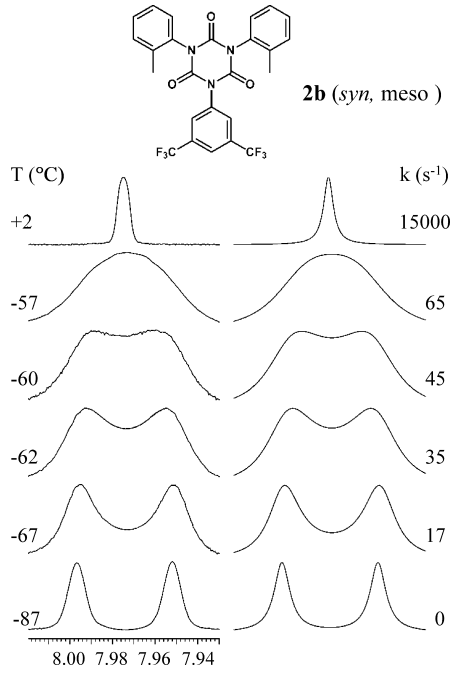

Figure 2. Left: temperature dependence of the signal of the 2,6 hydrogens of the 3,5-bis(trifluoromethyl)phenyl substituent of the second eluted diastereoisomer **2b** in CD_2Cl_2 at 600 MHz. Right: simulation obtained with the rate constants reported.

the equilibrium (**2b**:**2a** = 52:48) since the two isomers can be considered, within the experimental uncertainty, to be almost equally populated.

On the basis of this assignment, the isolated racemic diastereoisomer *anti* **2a** is expected to show two HPLC peaks when using an enantioselective chromatographic column, in that two enantiomers (atropisomers) can be separated.

This was actually verified, as shown in Figure S3 of the Supporting Information, where a cellulose-based enantioselective column was employed. The two atropisomers were isolated by semipreparative HPLC, and the second eluted yielded the electronic circular dichroism (ECD) spectrum displayed in Figure 3 (top). This spectrum was theoretically reproduced by assuming the configuration *M*,*M*. For this purpose, use was made of TD-DFT calculations, because this approach has been successfully employed several times to assign the absolute configuration of complex organic molecules.[20] In the present case, the simulation of the ECD spectrum is relatively straightforward in that only one conformation has to be taken into account owing to the rigidity of the system. Also, the vibrational circular dichroism (VCD)[21] spectrum of the same atropisomer was obtained in the region of the carbonyl absorption, and again, the experimental trace was satisfactorily simulated by assuming the same *M*,*M* configuration (Figure 3, bottom), thus making even more reliable the assignment of the *M*,*M* absolute configuration to the second eluted atropisomer of **2a**. Both the ECD and the VCD traces of the first eluted **2a** atropisomer displayed opposite phased spectra with respect to those of Figure 3, thus assigning the *P*,*P* configuration to this atropisomer.

To check whether the behavior observed in **2** might be somewhat affected by the electronic properties of the Ar_1 substituent, compound **3** (where Ar_1 is a *para*-methoxyphenyl group as in Scheme 1) was investigated. As in the case of **2**, two stable diastereoisomers were obtained, the ratio being 40:60.

dx.doi.org/10.1021/jo300192n | J. Org. Chem. 2012, 77, 3373−3380

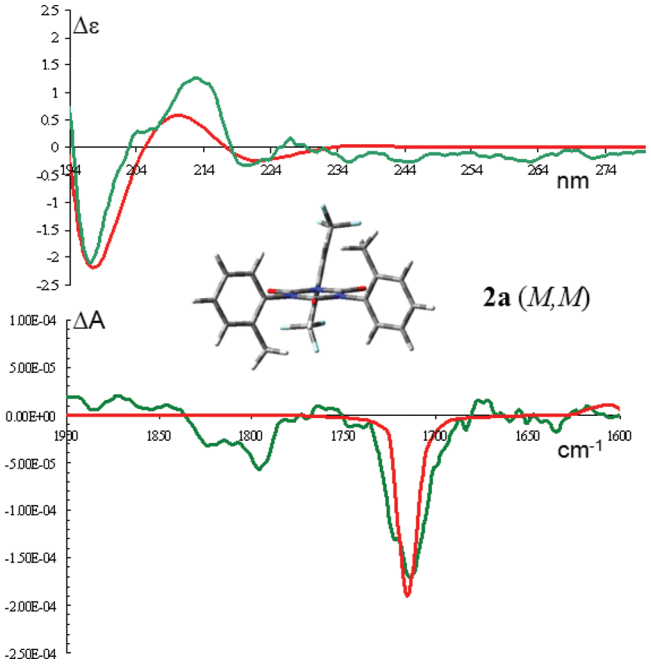

Figure 3. Top: experimental ECD spectrum (in CH_3CN) of the second eluted atropisomer of **2a** (green trace) and TD-DFT simulation (red trace, CAM-B3LYP/6-311++G(2d,p), shifted by +7 nm) assuming the absolute *M*,*M* configuration. Bottom: experimental VCD spectrum (in CCl_4) of the carbonyl region of the same atropisomer (green trace) and DFT simulation (red trace, B3LYP/6-31+G(2d,p), shifted by −45 nm) assuming the same *M*,*M* configuration.

The low-temperature ^{13}C spectrum of such a mixture showed that the major signal of the carbons *meta* to the *para*-methoxy group splits into two at −67 °C, whereas the corresponding minor signal does not. As discussed above for the case of **2**, this proves that the major diastereoisomer (labeled **3b**) corresponds to the *syn* (meso) and the minor (**3a**) to the *anti* (racemic) structure. The line-shape simulation (Figure S4 of the Supporting Information) afforded a $\Delta G^{\ddagger}$ value of 12.2 kcal mol^{-1} for the $N-Ar_1$ rotation barrier (DFT computation had predicted 10.8 kcal mol^{-1} for this process, as in Table 1). The barrier measured in **3b** is 1.4 kcal mol^{-1} higher than the corresponding barrier measured in **2b**. As a possible explanation, the electron-withdrawing properties of the CF_3 group substituent in **3** might favor the conjugation of the lone pair of the nitrogen with the aryl ring in the planar transition state of **2b**, lowering the energy of the transition state and thus reducing the corresponding rotational barrier. The experimental difference is rather small, but it is worth to outline that it is matched by the DFT calculations (predicted energy difference: 1.1 kcal mol^{-1}; experimental difference: 1.4 kcal mol^{-1}).

The major diastereoisomer **3b** (*syn*) was isolated and kept at +70 °C until the equilibrium with the minor **3a** (*anti*) was reached. At this temperature, the *anti*:*syn* ratio **3a**:**3b** (45:55) is quite close to that obtained in the synthetic procedure. The kinetic process was followed by monitoring the methyl NMR signals as a function of time, and the barrier for the interconversion of the major into the minor diastereoisomer was determined to be 26.8 kcal mol^{-1} (Figure S5 of the Supporting Information). This value compares well with the DFT computed value of 26.0 kcal mol^{-1} (Table 1). The two atropisomers of **3a** were separated by semipreparative enantioselective HPLC, and the first eluted atropisomer yielded the ECD spectrum and the VCD spectrum (in the region of the carbonyl absorption)[21] displayed in Figure S6 of the Supporting Information. By making use of the aforementioned TD-DFT and DFT approaches, respectively, these spectra were theoretically reproduced by assuming the absolute configuration *P*,*P*.

In the course of the purification of **3**, another derivative, bearing two *para*-methoxyphenyl substituents (compound **4** of Scheme 1), was also isolated (see the Experimental Section). Contrary to the cases of compounds **1**−**3**, compound **4** cannot yield configurationally stable diastereomeric forms, owing to the low rotation barrier of the *para*-methoxyphenyl groups, and it exists, consequently, as a single isomer. The barrier to rotation of the *para*-methoxyphenyl moiety was again determined by low-temperature NMR (Figure S7 of the Supporting Information), and essentially the same value as that of **3** was obtained (Table 1).

Compound **4** yielded single crystals suitable for X-ray diffraction so that an experimental structure could be obtained. As reported in the case of an analogous triphenyl isocyanurate,[22] the planes of the three aryl rings are indeed almost orthogonal with respect to that of the isocyanurate ring, as predicted by computations (Figure 4). This provides further support to the reliability of the DFT calculations used in the present investigation.

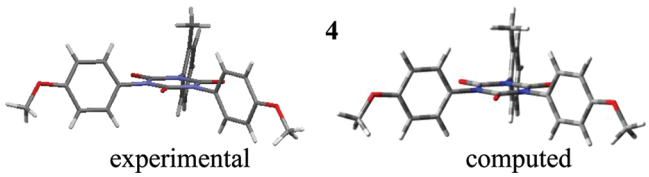

Figure 4. Experimental X-ray diffraction (left) and DFT computed structure (right) of compound **4**.

On the other hand, three diastereoisomers are expected to occur when one of the three C═O groups of **1** is substituted by a C═S moiety to yield compound **5**. The corresponding structures are indicated as *syn* (meso) **5a**, *anti* (meso) **5b**, and *anti* (racemic) **5c** (Scheme 3).

Scheme 3. Schematic Representation of the Stereoisomers of 5[a]

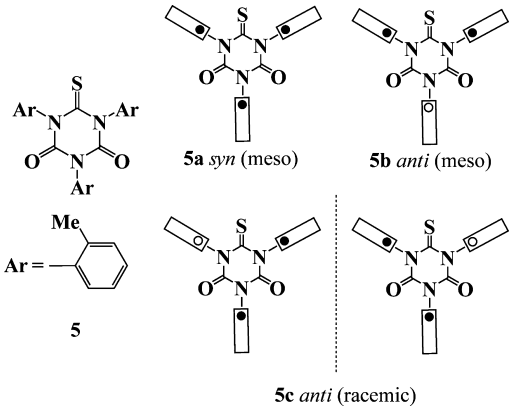

[a]The full and hollow dots indicate the position of the methyls above or under the plane of isocyanurate.

dx.doi.org/10.1021/jo300192n | J. Org. Chem. 2012, 77, 3373−3380

The synthetic procedure (see the Experimental Section) actually afforded three diastereoisomers that were separated by HPLC, the ratio being 39:18:43. The structure **5c** was assigned to the major diastereoisomer (43%) since it displays three NMR methyl signals with the same intensity, whereas both the other two (**5a** and **5b**) display two NMR methyl signals, each with a 2:1 intensity ratio.

To assign the latter structures, we resorted to NOE experiments. In the case of the minor diastereoisomer (18%), irradiation of the more intense of the two methyl signals did not yield any enhancement of the other methyl signal (and vice versa). Therefore, the minor isomer must have the *anti* (meso) structure **5b** where the two isochronous (enantiotopic) methyl groups are remote from the third one. On the contrary, the same experiment resulted in a large enhancement in the case of the 39% diastereoisomer (Figure S8 of the Supporting Information), indicating that its structure is *syn* (meso) **5a**, because the two isochronous (enantiotopic) methyl groups are located on the same face as the third methyl and are thus quite close.

When a solution of each isolated diastereoisomer was kept at high temperature (+110 °C in $C_2D_2Cl_4$) for a sufficiently long time, both the other two diastereoisomers were generated and the ratio measured at the equilibrium (**5a**:**5b**:**5c** = 39:19:42) turned out to be the same as that obtained by the reaction. When the separation was carried out using an enantioselective HPLC column, four peaks were observed because the peak corresponding to the racemic diastereoisomer **5c** (42%) splits into two since two atropisomers are present (~21% each, Figure S9 of the Supporting Information).

It has been reported[23] that, in the thiocarbonyl compounds, the UV and ECD bands are noticeably shifted to the red, and this feature makes the simulations more reliable because the absorption bands are far away from those of the solvent (acetonitrile).

The first eluted of the two atropisomers of **5c** provided the ECD spectrum displayed in Figure 5, which was very well reproduced, using the TD-DFT approach and assuming the *M,M* absolute configuration. In the present case, the ECD spectrum is more intense with respect to that of the corresponding carbonyl derivatives; thus the simulation is even more reliable.

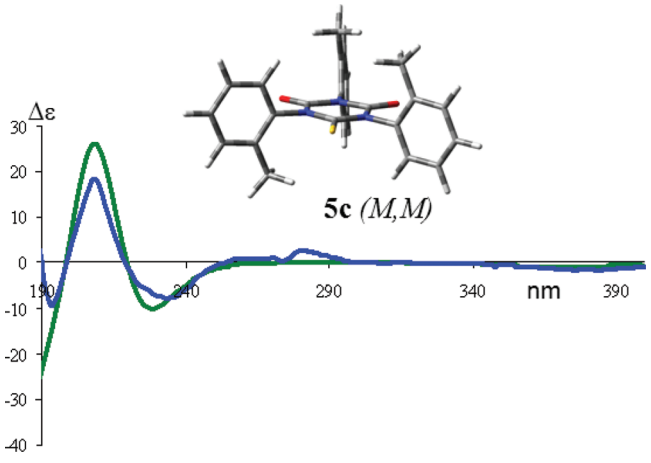

Figure 5. Experimental ECD spectrum (in CH_3CN) of the first eluted atropisomer of **5c** (blue trace) and TD-DFT computed simulation (green trace) obtained assuming the absolute *M,M* configuration.

CONCLUSIONS

It has been shown that isocyanurates can generate pairs of atropisomes owing to the hindered rotation about the N−aryl bond, even in the presence of small *ortho* substituents in the aryl ring, such as the methyl group. The availability to prepare isocyanurates containing two or three different aryl rings could be interesting for the preparation of a wide class of chiral diastereoisomers.

EXPERIMENTAL SECTION

Materials. The synthesis of isocyanurates **1**−**4** was carried out according to a procedure previously reported.[24]

1,3,5-Tri-o-tolyl-1,3,5-triazinane-2,4,6-trione (1). 1-Isocyanato-2-methylbenzene (0.13 g, 0.12 mL, 1 mmol) was heated at +130 °C in the presence of a catalytic quantity of potassium acetate until a white solid was obtained. After cooling at ambient temperature, the organic layer was diluted with CH_2Cl_2 and filtered on silica to remove the catalyst. The solvent was evaporated and the crude purified by semipreparative HPLC on a Kromasil-C18 (250 × 10 mm, 5 μm, CH_3CN/H_2O 7:3 v/v, 5 mL/min) to obtain the (*anti*) **1a** (0.089 g) and (*syn*) **1b** (0.033 g) as amorphous solids. Compound **1**: HRMS(EI) *m/z* calcd for $C_{24}H_{21}N_3O_3$: 399.1583. Found: 399.1587.

1a (*anti*): ^{1}H NMR (600 MHz, CD_3CN, 1.94 ppm, +25 °C): δ 2.30 (6H, s), 2.32 (3H, s), 7.31−7.37 (3H, m), 7.37−7.40 (6H, m), 7.40−7.44 (3H, m). ^{13}C NMR (CD_3CN, 118.2 ppm, +25 °C): δ 17.1 (2 CH_3), 17.3 (CH_3), 127.6 (1 CH), 127.7 (2 CH), 129.4 (2 CH), 129.5 (1 CH), 130.2 (3 CH), 131.5$_7$ (2 CH), 131.6$_1$ (1 CH), 134.0 (1 Cq), 134.1 (2 Cq), 137.1 (2 Cq-N), 137.4 (1 Cq-N), 148.9 (1 C═O), 149.1 (2 C═O).

1b (*syn*): ^{1}H NMR (600 MHz, CD_3CN, 1.94 ppm, +25 °C): δ 2.28$_5$ (9H, s), 7.34−7.42 (12H, m). ^{13}C NMR (150.8 MHz, CD_3CN, 118.2 ppm, +25 °C): δ 17.4 (3 CH_3), 128.2 (3 CH), 129.7 (3 CH), 130.6 (3 CH), 131.9 (3 CH), 134.6 (3 Cq), 137.2 (3 Cq-N), 149.3 (3 C═O).

1-(3,5-Bis(trifluoromethyl)phenyl)-3,5-di-o-tolyl-1,3,5-triazinane-2,4,6-trione (2). A mixture of 1-isocyanato-2-methylbenzene (0.13 g, 0.12 mL, 1 mmol) and 1-isocyanato-3,5-bis(trifluoromethyl)benzene (0.25 g, 0.17 mL, 1 mmol) was heated at +130 °C in the presence of a catalytic quantity of potassium acetate until a white solid was obtained. After cooling at room temperature, the organic layer was diluted with CH_2Cl_2 and filtered on silica to remove the catalyst. The solvent was evaporated and the crude purified by preparative HPLC on a Synergy Polar-RP (250 × 20 mm, 4 μm, CH_3CN/H_2O 8:2 v/v, 20 mL/min) to obtain 0.020 g of (**2**). HRMS(EI) *m/z* calcd for $C_{25}H_{17}N_3O_3F_6$: 521.1174. Found: 521.1185.

The pure meso **2b** (53%) and both the enantiomers of **2a** (47%) were isolated by enantioselective HPLC chromatography on a Chiralcel AD-H column (250 × 20 mm, 5 μm, hexane/*i*PrOH 98:2 v/v, 20 mL/min).

2b (meso): amorphous solid. ^{1}H NMR (600 MHz, CD_3CN, 1.94 ppm, +25 °C): δ 2.34 (6H, s), 7.34−7.43 (8H, m), 8.15 (3H, s). ^{13}C NMR (150.8 MHz, CD_3CN, 118.2 ppm, +25 °C): δ 17.5 (2 CH_3), 123.9 (2 CF_3, q, $^1J_{CF}$ = 271.4 Hz), 124.3 (CH_{para}, sept, $^3J_{CF}$ = 3.86 Hz), 128.1 (2 CH), 129.7 (2 CH), 130.6 (2 CH), 131.0 (2 CH_{orto}, q, $^3J_{CF}$ = 3.06 Hz), 132.0 (2 CH), 132.96 (2 Cq, q, $^2J_{CF}$ = 34.2 Hz), 134.3 (2 Cq), 137.2 (1 N-Cq), 137.6 (2 N-Cq), 148.9 (1 C═O), 149.4 (2 C═O). ^{19}F NMR (564.2 MHz, CD_3CN, $CFCl_3$, +25 °C): δ −63.81 (6F).

2a (racemic): amorphous solid. ^{1}H NMR (600 MHz, CD_3CN, 1.94 ppm, +25 °C): δ 2.33 (6H, s), 7.33−7.44 (8H, m), 8.15 (3H, s). ^{13}C NMR (150.8 MHz, CD_3CN, 118.2 ppm, +25 °C): δ 17.6 (2 CH_3), 123.9 (2 CF_3, q, $^1J_{CF}$ = 271.8 Hz), 124.2 (CH_{para}, sept, $^3J_{CF}$ = 3.96 Hz), 128.0 (2 CH), 129.7 (2 CH), 130.6 (2 CH), 131.0 (2 CH_{orto}, q, $^3J_{CF}$ = 3.64 Hz), 131.9 (2 CH), 132.95 (2 Cq, q, $^2J_{CF}$ = 34.2 Hz), 134.4 (2 Cq), 137.2 (1 N-Cq), 137.8 (2 N-Cq), 149.0 (1 C═O), 149.4 (2 C═O). ^{19}F NMR (564.2 MHz, CD_3CN, $CFCl_3$, +25 °C): δ −63.83 (6F).

1-(4-Methoxyphenyl)-3,5-di-o-tolyl-1,3,5-triazinane-2,4,6-trione (3) and 1,3-Bis(4-methoxyphenyl)-5-o-tolyl-1,3,5-triazinane-2,4,6-trione (4). A mixture of 1-isocyanato-2-methylbenzene (0.13 g, 0.12 mL, 1 mmol) and 1-isocyanato-4-methoxybenzene (0.15 g, 0.13 mL, 1

dx.doi.org/10.1021/jo300192n | J. Org. Chem. 2012, 77, 3373−3380

mmol) was heated at +130 °C in the presence of a catalytic amount of potassium acetate until a white solid was obtained. After cooling at room temperature, the organic layer was diluted with CH_2Cl_2 and filtered on silica to remove the catalyst. The solvent was evaporated and the crude purified by semipreparative HPLC on a Kromasil-C18 (250 × 10 mm, 5 μm, CH_3CN/H_2O 7:3 v/v, 5 mL/min) to obtain 0.060 g of (**4**) and 0.035 g of (**3**). The latter has HRMS(ESI-Orbitrap) *m*/*z* calcd for $C_{24}H_{22}N_3O_4^+$ $[M + H]^+$: 416.1605. Found: 416.1607.

The pure meso **3b** (60%) and both the enantiomers of **3a** (40%) were separated by enantioselective HPLC chromatography on a chiralcel AD-H column (hexane/*i*PrOH 98:2 v/v, 20 mL/min).

3b (meso): amorphous solid. ^{1}H NMR (600 MHz, CD_3CN, 1.94 ppm, +25 °C): δ 2.30 (6H, s), 3.84 (3H, s), 7.05−7.08 (2H, m), 7.33−7.44 (10H, m). ^{13}C NMR (150.8 MHz, CD_3CN, 118.2 ppm, +25 °C): δ 17.4_5 (2 CH_3), 56.1 (1 CH_3), 115.3 (2 CH), 127.9_5 (2 CH), 128.1 (1 N-Cq), 129.7_4 (2 CH), 130.4 (2 CH), 130.7 (2 CH), 131.8 (2 CH), 134.8 (2 Cq), 137.5 (2 N-Cq), 149.3 (1 C═O), 150.0 (2 C═O), 160.8_5 (1 MeO-Cq).

3a (racemic): amorphous solid. ^{1}H NMR (600 MHz, CD_3CN, 1.94 ppm, +25 °C): δ 2.31 (6H, s), 3.84 (3H, s), 7.04−7.08 (2H, m), 7.31−7.43 (10H, m). ^{13}C NMR (150.8 MHz, CD_3CN, 118.2 ppm, +25 °C): δ 17.6 (2 CH_3), 56.1 (1 CH_3), 115.3 (2 CH), 127.9 (2 CH), 128.2 (1 N-Cq), 129.8 (2 CH), 130.3 (2 CH), 130.7 (2 CH), 131.8 (2 CH), 134.9 (2 Cq), 137.8 (2 N-Cq), 149.3 (1 C═O), 150.0 (2 C═O), 160.8 (1 MeO-Cq).

*1,3-Bis(4-methoxyphenyl)-5-o-tolyl-1,3,5-triazinane-2,4,6-trione (**4**).* Crystalline solid. HRMS(ESI-Orbitrap) *m*/*z* calcd for $C_{24}H_{22}N_3O_5^+$ $[M + H]^+$: 432.1554. Found: 432.1543. ^{1}H NMR (600 MHz, CD_2Cl_2, 5.33 ppm, +25 °C): δ 2.31_5 (3H, s), 3.86_5 (6H, s), 7.04−7.07 (4H, m), 7.32−7.42 (8H, m). ^{13}C NMR (150.8 MHz, CD_2Cl_2, 53.67 ppm, +25 °C): δ 17.4 (1 CH_3), 55.7_6 (2 CH_3), 114.8 (4 CH), 126.6 (1 CH), 127.3_5 (2 N-Cq), 128.8_5 (1 CH), 129.7 (4 CH), 129.9 (1 CH), 131.4 (1 CH), 133.5 (1 Cq), 136.5 (1 N-Cq), 148.7 (2 C O), 149.5 (1 C═O), 160.3 (2 MeO-Cq). Single crystals suitable for X-ray diffraction were obtained by slow evaporation of a THF/CH_2Cl_2 solution (1:1 v/v).

*6-Thioxo-1,3,5-tri-o-tolyl-1,3,5-triazinane-2,4-dione (**5**).* Following a reported method,[25] 1,3,5-tri*o*-tolyl-1,3,5-triazinane-2,4,6-trione (**1**) (1 mmol = 400 mg) was reacted with 1.67 mmol of hexamethyldisiloxane and 0.183 mmol of P_4S_{10} in 1 mL of CH_2Cl_2 and heated to reflux overnight. After cooling at room temperature, the organic layer was eluted with CH_2Cl_2 and filtered on silica to remove the inorganic layer. The solvent was evaporated, and the crude (60.4%) was purified by semipreparative HPLC on a Luna-C18(2) column (250 × 20 mm, 5 μm, CH_3CN/H_2O 8:2, 20 mL/min). HRMS(ESI-Orbitrap) *m*/*z* calcd for $C_{24}H_{22}N_3O_2S^+$ $[M + H]^+$: 416.1427. Found: 416.1419. Separation of the four steroisomers (the two *meso* forms **5a** and **5b** and the two enantiomers of **5c**) was achieved by enantioselective HPLC chromatography on a Lux Cellulose-2 column (250 × 10 mm, 5 μm, hexane/*i*PrOH 90:10 v/v, 4 mL/min), as in Figure S9 of the Supporting Information

5a (*syn*, meso) (39%): amorphous solid. ^{1}H NMR (600 MHz, CD_3CN, 1.94 ppm, +25 °C): δ 2.26 (6H, s), 2.28 (3H, s), 7.35−7.42 (12H, m). ^{13}C NMR (150.8 MHz, CD_3CN, 118.2 ppm, +25 °C): δ 17.3 (2 CH_3), 17.4 (1 CH_3), 128.2_5 (1 CH), 128.3 (2 CH), 129.4 (2 CH), 129.5 (1 CH), 130.3 (2 CH), 130.7 (1 CH), 131.9 (2 CH), 131.9 (1 CH), 134.3 (1 Cq), 136.6 (2 Cq), 136.9 (1 Cq-N), 138.9 (2 N-Cq), 147.9 (2 C═O), 178.8 (1 C═S).

5b (*anti*, meso) (18.0%): amorphous solid. ^{1}H NMR (600 MHz, CD_3CN, 1.94 ppm, +25 °C): δ 2.30 (6H, s), 2.33_5 (3H, s), 7.36−7.41 (12H, m). ^{13}C NMR (150.8 MHz, CD_3CN, 118.2 ppm, +25 °C): δ 17.4 (2 CH_3), 17.7 (1 CH_3), 127.9_7 (1 CH), 128.0 (2 CH), 129.5 (2 CH), 129.7 (1 CH), 130.2 (2 CH), 130.7 (1 CH), 131.9 (2 CH), 132.0 (1 CH), 134.2_5 (1 Cq), 137.0 (2 Cq), 137.7 (1 Cq-N), 139.0 (2 NN-C), 147.9 (2 C═O), 178.8 (1 C═S).

5c (*anti*, racemic) (43%): amorphous solid. ^{1}H NMR (600 MHz, CD_3CN, 1.94 ppm, +25 °C): δ 2.30 (3H, s), 2.31 (3H, s), 2.33 (3H, s), 7.33−7.42 (11H, m), 7.46 (1H, d, *J* = 7.63 Hz). ^{13}C NMR (150.8 MHz, CD_3CN, 118.2 ppm, +25 °C): δ 17.4 (CH_3), 17.5 (CH_3), 17.7 (CH_3), 128.0 (1 CH), 128.1 (1 CH), 128.15 (1 CH), 129.59 (1 CH), 129.6 (2 CH), 130.2 (1 CH), 130.25 (1 CH), 130.6 (1 CH), 131.9 (1 CH), 131.95 (2 CH), 134.3 (1 Cq), 136.9 (1 Cq), 137.2 (1 Cq), 137.3 (1 N-Cq), 138.97 (1 N-Cq), 139.0 (1 N-Cq), 147.8 (1 C═O), 147.9 (1 C═O), 178.8 (1 C═S).

NMR Spectra. NMR spectra were recorded using a spectrometer operating at a field of 14.4 T (600 MHz for ^{1}H, 150.8 MHz for ^{13}C). Chemical shifts are given in parts per million relative to the internal standards tetramethylsilane (^{1}H and ^{13}C) and trichlorofluoromethane (^{19}F). The 600 MHz ^{1}H spectra were acquired using a 5 mm dual direct probe with a 9000 Hz spectral width, 2.0 μs (20° tip angle) pulse width, 3 s acquisition time, and 1 s delay time. A shifted sine bell weighting function[26] equal to the acquisition time (i.e., 3 s) was applied before the Fourier transformation. The 150.8 MHz ^{13}C spectra were acquired under proton-decoupling conditions with a 38 000 Hz spectral width, 4.2 μs (60° tip angle) pulse width, 1 s acquisition time, and 1 s delay time. A line-broadening function of 1−2 Hz was applied before the Fourier transformation. Assignments were obtained by means of the DEPT sequence. The 564.2 MHz ^{19}F spectra were acquired with a 100 kHz spectral width, 3 μs (30 tip angle) pulse width, 0.75 s acquisition time, and 1 s delay time.

The low-temperature spectra were obtained by using a flow of dry nitrogen that entered into an inox steel heat-exchanger immersed in liquid nitrogen and connected to the NMR probe head by a vacuum-insulated transfer line. Temperature calibrations were performed before the experiments, using a digital thermometer and a Cu/Ni thermocouple placed in an NMR tube filled with isopentane. The conditions were kept as equal as possible with all subsequent work. The uncertainty in the temperature measurements can be estimated from the calibration curve as ±2 °C.

Line-shape simulations were performed using a PC version of the QCPE DNMR6 program.[27] Electronic superimposition of the original and of the simulated spectra enabled the determination of the most reliable rate constants at a few different temperatures. These constants provided the free energies of activation ($\Delta G^{\ddagger}$) by means of the Eyring equation.[28] Within the experimental uncertainty, the latter values were found essentially invariant in the examined temperature range, thus implying an almost negligible activation entropy $\Delta S^{\ddagger}$, as observed in the majority of conformational processes investigated by dynamic NMR.[16b,29] The NOE experiments on **2** were performed as previously described,[16] those on **5** were obtained by means of the standard DPFGSE-NOE sequence.[30] To selectively irradiate the desired signal, a 50 Hz wide-shaped pulse was calculated with a refocusing-SNOB shape[31] and a pulse width of 37 ms. The mixing time was set to 1.5 s.

ECD and VCD spectra. Standard UV absorption spectra were recorded at +25 °C in acetonitrile on the racemic mixtures, in the 200−400 nm spectral region. ECD spectra were recorded at +24 °C in acetonitrile solutions, using a path length of 0.2 cm. Spectra were recorded in the range of 190−400 nm.

VCD spectra were recorded on a single-PEM Fourier transform spectrometer using a 4 cm^{-1} resolution. Spectra were recorded in $CDCl_3$ solutions in a BaF_2 cell (100 μm path length). The concentrations of the samples were calibrated to obtain an absorbance in the 0.5−0.7 range for the carbonyl signals; 10 000 scans were collected (3.5 h). The spectra were calibrated using the internal calibration files, based on the spectrum of neat (-)-α-pinene. Baseline artifacts were corrected by subtracting the VCD spectrum of the second eluted enantiomer to the spectrum of the first one. The final spectrum was then divided by 2 to obtain the correct Δ*A* intensity.

Calculations. A conformational search was preliminarily carried out by means of the molecular mechanics force field (MMFF), using the Monte Carlo method implemented in the package TITAN 1.0.5.[32] The most stable conformers thus identified were subsequently energy-minimized by DFT computations, which were performed by the Gaussian 09, rev. A.02, series of programs[33] using standard optimization parameters. All the calculations employed the B3LYP hybrid HF-DFT method[34] and the 6-31G(d) basis sets. Harmonic vibrational frequencies were calculated for all the stationary points. As revealed by the frequency analysis, imaginary frequencies were absent in all ground states, whereas one imaginary frequency was associated with each transition state. Visual inspection of the corresponding

dx.doi.org/10.1021/jo300192n | J. Org. Chem. 2012, 77, 3373−3380

normal mode[35] validated the identification of the transition states. The energy values of the barriers listed in Table 1 derive from total electronic energies. In general, these give the best fit with experimental DNMR data,[36] and for this reason, the computed values have not been corrected for zero-point energy contributions or other thermodynamic parameters. This approach avoids artifacts due to the ambiguous choice of the adequate reference temperature and from the idealization of low-frequency vibrators as harmonic oscillators.[37]

ECD and VCD Simulations. The ECD spectra of **2a**, **2c**, and **5** were simulated by means of TD-DFT calculations. The electronic excitation energies and rotational strengths have been calculated in the gas phase using the geometries obtained at the B3LYP/6-31G(d) level with the CAM-B3LYP functional that includes long-range correction using the Coulomb attenuating method.[38] All the calculations employed the 6-311++G(2d,p) basis set because this basis set has been widely used in this kind of calculation and proved to be sufficiently accurate at a reasonable computational cost. Rotational strengths were calculated in both length and velocity representation, the resulting values being very similar (differences below 5%). For this reason, the errors due to basis set incompleteness should be very small, or negligible.[39] The simulated spectra were obtained using the first 50 calculated transitions (lowest wavelength about 165 nm) and applying a 0.5 eV line width. The calculated VCD spectra were obtained by frequency calculations at the B3LYP/6-31+G(2d,p) level, using the optimized geometries obtained at the B3LYP/6-31G(d) level.

■ ASSOCIATED CONTENT

Supporting Information

Kinetics of the thermal equilibration of **1**−**3**; enantioselective HPLC traces of **2** and **5**; experimental and simulated VT ^{13}C NMR spectra of **3** and **4**; experimental and simulated ECD and VCD spectra of **3**; NOE spectra of **5**; ECD spectra of the enantiomeric pairs of **2**, **3**, and **5**; crystallographic data of **4**; ^{1}H and ^{13}C NMR spectra and DFT computational data of **1**−**5**. This material is available free of charge via the Internet at http://pubs.acs.org.

■ AUTHOR INFORMATION

Corresponding Author

*E-mail: andrea.mazzanti@unibo.it.

Notes

The authors declare no competing financial interest.

■ ACKNOWLEDGMENTS

Financial contribution was received from the University of Bologna (RFO funds 2009 and 2010).

■ REFERENCES

(1) Duong, H. A.; Cross, M. J.; Louie, J. *Org. Lett.* **2004**, *6*, 4679−4681.

(2) Lin, I. S.; Kresta, J. E.; Frisch, K. C. *Reaction Injection Molding and Fast Polymerization Reactions*; Plenum Publishing: New York, 1982; p 147.

(3) (a) Wirpsza, Z. *Polyurethanes: Chemistry, Technology and Application*; Ellis Horwood: London, UK, 1993. (b) Zitinkina, A. K.; Sibanova, N. A.; Tarakanov, O. G. *Russ. Chem. Rev.* **1985**, *54*, 1866. (c) Nawata, T.; Kresta, J. E.; Frisch, K. C. *J. Cell. Plast.* **1975**, 267−278. (d) Nicholas, L.; Gmitter, G. R. *J. Cell. Plast.* **1965**, 85−90.

(4) (a) Bukac, Z.; Sebenda, J. *Chem. Prum.* **1985**, *35*, 361. (b) Horsky, J.; Kubanek, U.; Marick, J.; Kralicek, J. *Chem. Prum.* **1982**, *32*, 599.

(5) (a) Misawa, H.; Koseki, T. Patent JP 03,166,255, 1991. (b) Hirabayashi, M.; Ozawa, S. Patent JP 0,309,907, 1991. (c) Sato, F.; Tateyama, M.; Kurokawa, S. Patent JP 63,122,748, 1988. (d) Ishikawa, T.; Tanaka, S.; Shidara, M.; Hatsurtori, I.; Takagame, H.; Mashita, K. Patent JP 0187,651, 1989. (e) Nagai, H.; Komya, T. Patent JP 0187,649, 1989. (f) Osturek, R.; Wingler, F.; Geyev, O. Patent DE 3,729,457, 1989.

(6) (a) Sugimoto, H.; Yamane, Y.; Inoue, S. *Tetrahedron: Asymmetry* **2000**, *11*, 2067−2075. (b) Murray, A. P.; Miller, M. J. *J. Org. Chem.* **2003**, *68*, 191−194. (c) Ghosh, M.; Miller, M. J. *J. Org. Chem.* **1994**, *59*, 1020−1026.

(7) Gust, D. *J. Am. Chem. Soc.* **1977**, *99*, 6980−6982.

(8) Gust, D.; Patton, A. *J. Am. Chem. Soc.* **1978**, *100*, 8175−8181.

(9) Harada, K.; Hart, H.; Du, C.-J. F. *J. Org. Chem.* **1985**, *50*, 6524−6528.

(10) Pepermans, H.; Willem, R.; Gielen, M.; Hoogzand, C. *J. Org. Chem.* **1986**, *51*, 301−306.

(11) Katz, H. E. *J. Org. Chem.* **1987**, *52*, 3932−3934.

(12) Dell'Erba, C.; Gasparrini, F.; Grilli, S.; Lunazzi, L.; Mazzanti, A.; Novi, M.; Pierini, M.; Tavani, C.; Villani, C. *J. Org. Chem.* **2002**, *67*, 1663−1668.

(13) Grilli, S.; Lunazzi, L.; Mazzanti, A.; Pinamonti, M. *Tetrahedron* **2004**, *60*, 4451−4458.

(14) Lunazzi, L.; Mazzanti, A.; Minzoni, M.; Anderson, J. E. *Org. Lett.* **2005**, *7*, 1291−1294.

(15) Lunazzi, L.; Mazzanti, A.; Minzoni, M. *J. Org. Chem.* **2005**, *70*, 10062−10066.

(16) (a) Lunazzi, L.; Mazzanti, A. *J. Am. Chem. Soc.* **2004**, *126*, 12155−12157. (b) Lunazzi, L.; Mancinelli, M.; Mazzanti, A. *J. Org. Chem.* **2007**, *72*, 5391−5394. (c) Lunazzi, L.; Mancinelli, M.; Mazzanti, A. *J. Org. Chem.* **2008**, *73*, 2198−2205. (d) Lunazzi, L.; Mancinelli, M.; Mazzanti, A. *J. Org. Chem.* **2009**, *74*, 1345−1348.

(17) The ^{13}CH coupling constants of the methyl groups in **2a** and **2b** are both equal to 127.5 Hz.

(18) The computed averaged interproton methyl distances are 4.08 Å in the case of the *syn* (meso) **2b** and 6.43 Å in the case of the *anti* (racemic) **2a**. As required when dealing with NOE experiments, these averages were obtained by taking into account the 6th root, according to Claridge, T. D. W. *High Resolution NMR Techniques in Organic Chemistry*; Pergamon: Oxford, UK, 1999; p 303. (If the 6th root is not applied, the corresponding averaged distances become 4.84 and 6.69 Å, respectively.)

(19) Owing to the unresolved long-range couplings with fluorine of CF_3, the *ortho* signals are too broad to display the multiplicity expected for the *J* coupling with the *meta* hydrogens and thus appear as single signals.

(20) (a) Lunazzi, L.; Mancinelli, M.; Mazzanti, A. *J. Org. Chem.* **2011**, *76*, 1487−1490. (b) Mazzeo, G.; Giorgio, E.; Zanasi, R.; Berova, N.; Rosini, C. *J. Org. Chem.* **2010**, *75*, 4600−4603. (c) Pescitelli, G.; Di Pietro, S.; Cardellicchio, C.; Annunziata, M.; Capozzi, M.; Di Bari, L. *J. Org. Chem.* **2010**, *75*, 1143−1154. (d) Jacquemin, D.; Perpète, E. A.; Ciofini, I.; Adamo, C.; Valero, R.; Zhao, Y.; Truhlar, D. G. *J. Chem. Theory Comput.* **2010**, *6*, 2071−2085. (e) Gioia, C.; Fini, F.; Mazzanti, A.; Bernardi, L.; Ricci, A. *J. Am. Chem. Soc.* **2009**, *131*, 9614−9615. (f) Stephens, P. J.; Pan, J. J.; Devlin, F. J.; Cheeseman, J. R. *J. Nat. Prod.* **2008**, *71*, 285−288. For reviews, see: (g) Bringmann, G.; Bruhn, T.; Maksimenka, K.; Hemberger, Y. *Eur. J. Org. Chem.* **2009**, 2717−2727. (h) Bringmann, G.; Gulder, T. A. M.; Reichert, M.; Gulder, T. *Chirality* **2008**, *20*, 628−642. (I) Berova, N.; Di Bari, L.; Pescitelli, G. *Chem. Soc. Rev.* **2007**, *36*, 914−931.

(21) (a) Stephens, P. J.; Aamouche, A.; Devlin, F. J.; Superchi, S.; Donnoli, M. J.; Rosini, C. *J. Org. Chem.* **2001**, *66*, 3671−3677. (b) Stephens, P. J.; Devlin, F. J. *Chirality* **2000**, *12*, 172−179. (c) Yabuchi, T.; Kusumi, T. *J. Am. Chem. Soc.* **1999**, *121*, 10646−10647. (d) Stephens, P. J. *J. Phys. Chem.* **1985**, *89*, 748−752. (e) Nafie, L. A.; Cheng, J. C.; Stephens, P. J. *J. Am. Chem. Soc.* **1975**, *97*, 3842−3843. For reviews, see: (f) Saflei, J.; Dobrowolsky, J. Cz. *Chem. Soc. Rev.* **2010**, *39*, 1478−1488. (g) Stephens, P. J.; Devlin, F. J.; Pan, J.-J. *Chirality* **2008**, *20*, 643−663. (h) Magyarfalvi, G.; Tarczay, G.; Vass, E. *Wiley Interdiscip. Rev.: Comput. Mol. Sci.* **2011**, *1*, 403−425.

(22) (a) Usanamaz, A. *Acta Crystallogr.* **1979**, *B35*, 1117−1119. (b) Mariyatra, M. B.; Panchanatheswaran, K.; Low, J. N.; Glidwell, C. *Cryst. Struct. Commun.* **2004**, *C60*, o682−o685.

(23) (a) Woźnica, M.; Butkiewicz, A.; Grzywacz, A.; Kowalska, P.; Masnyk, M.; Michalak, K.; Luboradzki, R.; Furche, P.; Kruse, H.; Grimme, S.; Frelek, J. *J. Org. Chem.* **2011**, *76*, 3306−3319. (b) Maciejewski, A.; Steer, R. P. *Chem. Rev.* **1993**, *93*, 67−98. (c) Kajtar, M.; Kajtar, J.; Maier, Z.; Zewdu, M.; Hollosi, M. *Spectrochim. Acta* **1993**, *48B*, 87−91.
(24) Kogon, I. C. *J. Am. Chem. Soc.* **1956**, *78*, 4911−4914.
(25) Cho, D.; Ahn, J.; De Castro, K.; Ahn, H.; Rhee, H. *Tetrahedron* **2010**, *66*, 5863−5588.
(26) Claridge, T. D. W. *High Resolution NMR Techniques in Organic Chemistry*; Pergamon: Oxford, UK, 1999; p 71.
(27) Brown, J. H.; Bushweller, C. H. *DNMR6: Calculation of NMR Spectra Subject to the Effects of Chemical Exchange, (program 633)*; QCPE Bulletin, Bloomington, IN; 1983; Vol. 3, pp 103−103. A copy of the program is available on request from the authors (L.L. and A.M.).
(28) Eyring, H. *Chem. Rev.* **1935**, *17*, 65−77.
(29) (a) Hoogasian, S.; Bushweller, C. H.; Anderson, W. G.; Kingsley, G. *J. Phys. Chem.* **1976**, *80*, 643−648. (b) Casarini, D.; Lunazzi, L.; Mazzanti, A. *Eur. J. Org. Chem.* **2010**, *75*, 2035−2056 and references quoted therein.
(30) (a) Stonehouse, J.; Adell, P.; Keeler, J.; Shaka, A. J. *J. Am. Chem. Soc.* **1994**, *116*, 6037−6038. (b) Stott, K.; Stonehouse, J.; Keeler, J.; Hwang, T. L.; Shaka, A. J. *J. Am. Chem. Soc.* **1995**, *117*, 4199−4200. (c) Stott, K.; Keeler, J.; Van, Q. N.; Shaka, A. J. *J. Magn. Reson.* **1997**, *125*, 302−324. (d) Van, Q. N.; Smith, E. M.; Shaka, A. J. *J. Magn. Reson.* **1999**, *141*, 191−194.
(31) Kupče, E.; Boyd, J.; Campbell, I. D. *J. Magn. Reson., Ser. B* **1995**, *106*, 300−303.
(32) *Package TITAN 1.0.5*; Wavefunction Inc.: Irvine, CA.
(33) Frisch, M. J.; Trucks, G. W.; Schlegel, H. B.; Scuseria, G. E.; Robb, M. A.; Cheeseman, J. R.; Scalmani, G.; Barone, V.; Mennucci, B.; Petersson, G. A.; Nakatsuji, H.; Caricato, M.; Li, X.; Hratchian, H. P.; Izmaylov, A. F.; Bloino, J.; Zheng, G.; Sonnenberg, J. L.; Hada, M.; Ehara, M.; Toyota, K.; Fukuda, R.; Hasegawa, J.; Ishida, M.; Nakajima, T.; Honda, Y.; Kitao, O.; Nakai, H.; Vreven, T.; Montgomery, J. A., Jr.; Peralta, J. E.; Ogliaro, F.; Bearpark, M.; Heyd, J. J.; Brothers, E.; Kudin, K. N.; Staroverov, V. N.; Kobayashi, R.; Normand, J.; Raghavachari, K.; Rendell, A.; Burant, J. C.; Iyengar, S. S.; Tomasi, J.; Cossi, M.; Rega, N.; Millam, N. J.; Klene, M.; Knox, J. E.; Cross, J. B.; Bakken, V.; Adamo, C.; Jaramillo, J.; Gomperts, R.; Stratmann, R. E.; Yazyev, O.; Austin, A. J.; Cammi, R.; Pomelli, C.; Ochterski, J. W.; Martin, R. L.; Morokuma, K.; Zakrzewski, V. G.; Voth, G. A.; Salvador, P.; Dannenberg, J. J.; Dapprich, S.; Daniels, A. D.; Farkas, Ö.; Foresman, J. B.; Ortiz, J. V.; Cioslowski, J.; Fox, D. J. *Gaussian 09*, revision A.02; Gaussian, Inc.: Wallingford, CT, 2009.
(34) (a) Lee, C.; Yang, W.; Parr, R. G. *Phys. Rev. B* **1988**, *37*, 785−789. (b) Becke, A. D. *J. Chem. Phys.* **1993**, *98*, 5648−5652. (c) Stephens, P. J.; Devlin, F. J.; Chabalowski, C. F.; Frisch, M. J. *J. Phys. Chem.* **1994**, *98*, 11623−11627.
(35) *Package GaussView 5.0.9*; Gaussian Inc.: Wallingford, CT, 2009.
(36) Ayala, P. Y.; Schlegel, H. B. *J. Chem. Phys.* **1998**, *108*, 2314−2325.
(37) (a) Wong, M. W. *Chem. Phys. Lett.* **1996**, *256*, 391−399. (b) Wheeler, S. E.; McNeil, A. J.; Müller, P.; Swager, T. M.; Houk, K. *J. Am. Chem. Soc.* **2010**, *132*, 3304−3311.
(38) Yanai, T.; Tew, D.; Handy, N. *Chem. Phys. Lett.* **2004**, *393*, 51−57.
(39) Stephens, P. J.; McCann, D. M.; Devlin, F. J.; Cheeseman, J. R.; Frisch, M. J. *J. Am. Chem. Soc.* **2004**, *126*, 7514−7521.